

Article

Study on the Preparation and Aging Performance of Temperature-Indicating Patch Used for Thermal Defect Detection of Transformer Bushing Cylinder Head

Mingqin Wang¹, Xiaobin Wu¹, Nan Jiang¹, Chenghua Liu¹, Richang Xian^{2,*} and Wentao Jia²

¹ State Grid Shandong Linyi Power Supply Company, Linyi 276000, China; ltysdut@163.com (M.W.); 19862513527@163.com (X.W.); sunwangruixiao@163.com (N.J.); alen_ncu@163.com (C.L.)

² College of Electrical and Electronic Engineering, Shandong University of Technology, Zibo 255000, China; tajwt888@163.com

* Correspondence: xianrc@163.com

Abstract: Elevated temperatures at the transformer bushing cylinder head can precipitate failures, leading to significant power outages. In response, this study introduces a reversible temperature-indicating patch for the nuanced detection of thermal anomalies in the transformer bushing's cylinder head. The patch, crafted through a melting process, utilizes a reversible discoloration material and is developed in two variants via an adsorption substrate method. Comprehensive evaluations of the patches' color-changing characteristics, alongside their electrical and hydrophobic properties, were conducted using an automatic contact angle measuring instrument and an AC flashover test platform. The findings reveal that the temperature-indicating patch exhibits a discernible color transition within the range of 49~55 °C, with a color reversion temperature span of 45~55 °C, denoting marked sensitivity and robust reversibility. Additionally, it was observed that prolonged thermal aging correlates with a decrease in both the water contact angle and the discharge voltage per unit length across the surface of the patches, indicating a degradation in performance. Among the variants, the binder-based temperature-indicating patch demonstrated superior stability in electrical performance compared to its vacuum-based counterpart. The outcomes of this research offer valuable insights for the development of advanced diagnostic tools for the identification of thermal defects in transformer bushings, potentially enhancing reliability and safety in power distribution systems.

Keywords: transformer bushing cylinder head; temperature-indicating patch; color-changing properties; thermal aging



Citation: Wang, M.; Wu, X.; Jiang, N.; Liu, C.; Xian, R.; Jia, W. Study on the Preparation and Aging Performance of Temperature-Indicating Patch Used for Thermal Defect Detection of Transformer Bushing Cylinder Head. *Processes* **2024**, *12*, 736. <https://doi.org/10.3390/pr12040736>

Academic Editor: Michael C. Georgiadis

Received: 6 March 2024

Revised: 27 March 2024

Accepted: 27 March 2024

Published: 4 April 2024



Copyright: © 2024 by the authors. Licensee MDPI, Basel, Switzerland. This article is an open access article distributed under the terms and conditions of the Creative Commons Attribution (CC BY) license (<https://creativecommons.org/licenses/by/4.0/>).

1. Introduction

Transformer bushings are pivotal for introducing leads and providing insulation from the ground, while also securing and stabilizing these leads. They must meet stringent criteria for electrical and mechanical durability, thermal resilience, and maintenance accessibility. The failure of a transformer bushing can precipitate disruptions in the power network and raise significant safety concerns [1–4]. Consequently, the upkeep and comprehensive inspection of transformer bushings are of paramount importance. Subject to variations in seasonal demand, these bushings endure heightened stress, expediting wear and tear and potentially catalyzing failures that result in grid outages [5–7]. The research shows that the probability of heating failure at the top of the transformer bushing in practical applications is large, and the main reasons are as follows: (1) loose joint: due to the looseness of the joint connecting the transformer bushing and the guide wire, the contact area decreases, the contact resistance increases, and a lot of heat is generated, resulting in a high temperature at the wiring; (2) overload: when the transformer bushing bears too much load current, it will cause the temperature at the wiring point to be too high; (3) uneven conductor surface: an uneven conductor surface or foreign bodies on the conductor surface will also lead to

poor contact, making the contact resistance increase, generating a lot of heat, resulting in high temperature at the wiring; (4) environmental factors: the ambient temperature of the transformer is too high; poor ventilation and other environmental factors will also lead to overheating of the joint. Therefore, it is of great significance to study the temperature detection of the top cylinder of transformer bushings.

Methods for monitoring the temperature of transformer bushings include direct measurement methods and indirect calculation methods. The direct measurement methods are mainly infrared, thermal resistance, thermocouple, and distributed optical fiber techniques, as well as a temperature-measuring wax sheet [8–11]. The indirect measurement methods mainly include the national standard calculation method and numerical calculation method [12]. Infrared methods, advantageous for their non-contact nature and long-distance applicability, offer rapid response times yet are influenced by surface emissivity and environmental conditions. Thermal resistance methods, while boasting high accuracy and stability, necessitate regular calibration due to their slower response. Despite its affordability and broad measurement range, thermal resistance is prone to degradation from oxidation and corrosion. Distributed optical fiber technology, recognized for its precision and immunity to electromagnetic interference, remains cost-prohibitive for widespread adoption. The temperature-indicating wax sheet can reflect the thermal fault defects of power equipment in real time, and it is low in price and simple in structure. However, it is not reversible and needs to be replaced frequently, which increases the operation and maintenance cost. The national standard calculation method has the characteristics of being a simple calculation and easy to implement, but its calculation accuracy is poor. The results of the numerical calculation method are intuitive, and the temperature distribution inside the transformer can be obtained, but the computer hardware requirements are high and the cost is high.

Emerging research focuses on thermochromic materials for their sensitivity and versatility, presenting novel approaches for bushing temperature assessment [13–15]. Innovations include thermally reversible color-changing coatings developed by Dong Bingbing, designed for identifying thermal anomalies in dry-type air-core reactors [16]; and Chen Yuanyuan's irreversible temperature-indicating coatings aimed at pinpointing lightning fault locations, facilitating temperature distribution analysis, and monitoring equipment for overheating [17]. Wang Peng used room temperature vulcanized silicone rubber mixed with thermochromic microcapsules and nano-silica to prepare the superhydrophobic intelligent color-changing coating, which realized the consideration of thermochromic, superhydrophobic, and surface discharge performance [18]. Zhou Ronghua used thermoplastic acrylic resin as the base material to prepare thermochromic color-changing paint that can be used for ABS plastic substrate, comprehensively discussed and analyzed the factors affecting the color-changing temperature of the thermochromic paint, and optimized the paint, finally preparing a one-component thermotemperature-reversible thermochromic color-changing paint with good performance and convenient construction [19]. Rahul Bhattacharya combined the gain and loss mechanisms of crystal water to detect the temperature. $(\text{CHN}_2)\text{CuCl}_4$ absorbed water to form a green hydrate $(\text{CHN}_2)\text{CuCl}_4 \cdot \text{H}_2\text{O}$, it then lost crystal water to form $(\text{CHN}_2)_2\text{CuCl}_4$ when the temperature rose to about 43 °C. The color changed from green to yellow. When the temperature was lowered, green water and $(\text{CHN}_2)\text{CuCl}_4 \cdot \text{H}_2\text{O}$ were formed again after water absorption [20]. The standard DL/T 664-2016 states that a transformer casing cylinder head temperature of 55 °C is a serious defect [21], but there is no research on defect temperature detection in transformer casing cylinder heads at present. In addition, the color-changing paint has the disadvantage of poor aging performance, and the temperature-indicating patch has good stability and is less affected by environmental factors. Based on this, research on a reversible temperature-indicating patch on the cylinder head of the transformer bushing is carried out.

This study presents the synthesis of reversible color-changing materials via a melting process, leading to the fabrication of two distinct types of temperature-indicating patches. Utilizing a cellulose–polyester blend fabric as the absorptive base, we developed both binder-based and vacuum-based temperature-indicating patches. These innovations were rigorously evaluated for their chromatic transitions, electrical characteristics, and water-repellent properties. The findings of this research offer valuable insights for the advancement of thermal defect detection methodologies in transformer bushings, potentially setting new benchmarks for diagnostic accuracy and reliability.

2. Test Part

2.1. Test Reagents and Instruments

Test reagents: crystalline violet lactone (Nanjing Bermuda Biotechnology Co., Ltd., Nanjing, China); bisphenol A (Shandong Zhengxing New Materials Co., Ltd., Jinan, China); octadecanol (Sinopharm Group Chemical Reagent Co., Ltd., Shanghai, China); Polyethylene Terephthalate (PET) film (Shenzhen Zhenhua Adhesive Products Co., Ltd., Shenzhen, China); sealed bag (Dongguan Yiguang Packaging Machinery Co., Ltd., Dongguan, China); binder (Anhui Maoyuan Co., Ltd., Hefei, China).

Test instruments: constant-temperature heating magnetic stirrer (110 V; Shanghai Iohua Instrument Co., Ltd., Shanghai, China); constant-temperature heating table (Dongguan Weitieke Automation Technology Co., Ltd., Dongguan, China).

2.2. Sample Preparation

2.2.1. Preparation of Color-Changing Materials

This study utilized the melting process to synthesize color-changing materials, employing crystalline violet lactone, bisphenol A, and octadecanol as primary raw materials. The proportions of crystalline violet lactone, bisphenol A, and octadecanol were meticulously calculated based on a mass ratio of 1:2:50. Initially, octadecanol was placed in a beaker and subjected to heating using a constant temperature magnetic stirrer, with the temperature precisely set to 80 °C. Upon complete melting of the octadecanol, crystalline violet lactone and bisphenol A were sequentially introduced, ensuring thorough mixing and homogenization at a stirring speed of 500 revolutions per minute (rpm). This mixture was continuously heated and stirred for 60 min. Following a 24 h period of natural cooling, the resultant solidified blue color-changing material was finely ground into a powder form.

2.2.2. Preparation of Reversible Thermochromic Patches

This research delineates the fabrication of two variants of oscillometric patches, binder-type and vacuum-based, with the preparation process shown in Figure 1. Initially, a specified quantity of the previously synthesized color-changing powder was heated until molten in a beaker. A cellulose–polyester blend fabric, serving as the adsorption substrate, was then thoroughly saturated in the molten mixture, subsequently extracted, and placed into custom pressing molds. For the binder-type oscillometric patches, a uniform layer of binder was applied to one side of a PET film, which, upon pressure molding, ensured a secure adhesion to the aluminum substrate plate. This process eliminated air pockets, resulting in the formation of binder-type temperature-responsive patch samples. Conversely, the vacuum-based patches were produced by enclosing the cooled and pressed material within a high-temperature sealing bag and subjecting it to vacuum sealing. A binder was then applied to facilitate adherence to the aluminum substrate plate, culminating in the creation of vacuum-based temperature-responsive patch samples. These samples were specifically designed for the detection of thermal anomalies in the bushing columns of transformers.

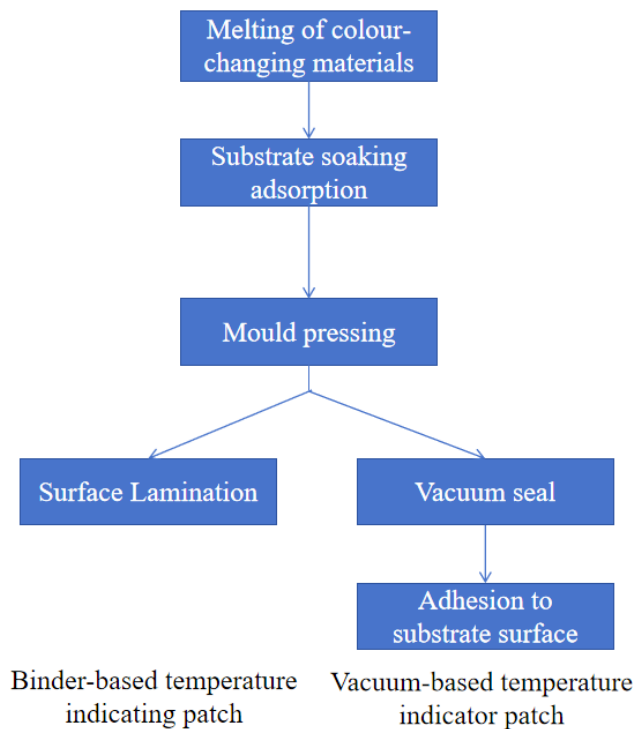


Figure 1. Preparation process of temperature indicator patch.

2.3. Test Methods

2.3.1. Color-Changing Performance of Temperature-Indicating Patch

The temperature indicator patch prepared in this test for thermal defect detection in transformer bushing cylinder heads tests the following parameters [22,23]:

(1) Discoloration temperature: The experiment commenced with the placement of the temperature-sensitive patch, adhered to a substrate, on a precision-controlled heating platform. The platform's initial temperature was meticulously set to 30 °C. Employing a graduated heating approach, the temperature was incrementally increased by 1 °C every three minutes. Throughout this process, the chromatic transition of the patch was systematically documented, establishing a detailed profile of its temperature responsiveness.

(2) Fading time: For this analysis, the heating platform upon which the test specimen was positioned was stabilized at 70 °C. Utilizing high-resolution videography, the chromatic evolution of the specimen was captured in real time. The onset of the color transformation was marked at zero seconds, and the interval required for the patch to undergo complete discoloration was precisely measured, defining the fading time.

(3) Recoloring time: Following the complete discoloration, the specimen was immediately subjected to ambient conditions to facilitate natural cooling. The recoloration process was recorded in real time using high-definition video capture. The recoloring time was calculated from the moment local color restoration commenced (marked as zero seconds) to the point of full chromatic recovery.

(4) Color representation: According to CIE 1976 $L^*a^*b^*$ uniform color space, a lab color space model was used to represent the color change of the temperature patch, namely, the brightness index (L), red–green axis chromaticity index (a), and yellow–blue axis chromaticity index (b). The colorimetric parameters of the complex state (L_1, a_1, b_1) and faded state (L_2, a_2, b_2) were extracted, and the color difference ΔE was calculated.

$$\Delta E = \sqrt{\Delta L^2 + \Delta a^2 + \Delta b^2} = \sqrt{(L_1 - L_2)^2 + (a_1 - a_2)^2 + (b_1 - b_2)^2}$$

In the formula, ΔL , Δa , Δb are the differences between the colorimetric parameters before and after the discoloration of the discoloration material.

2.3.2. Thermal Patch Aging Test

(1) Thermal aging protocol: The study implemented a thermal aging assessment based on the guidelines set forth in GB 11026.1-1989 [24], which provides a framework for determining the heat resistance of electrical insulation materials, including the formulation of aging test methods and the interpretation of test results. The temperature-indicating patches were subjected to an accelerated aging process within a constant temperature chamber, set to maintain an aging temperature of 80 °C. The evaluation was conducted by averaging the results across three distinct test batches to ensure reliability and statistical significance.

(2) Insulation performance analysis: Insulation integrity was assessed utilizing the surface flashover test principle, as depicted in Figure 2. The test circuit consisted of a console, protection resistor, test transformer, and capacitor divider. The oscilloscope was connected to a high-voltage probe to detect the output voltage in real time. This examination was conducted under controlled environmental conditions, maintained at (25 ± 1) °C. Adhering to the standards outlined in GB/T 1408.1-2016 [25], a gradual-voltage-increase test was employed, with a voltage ramp rate meticulously set to 0.5 kV/s. This method ensures a comprehensive evaluation of the insulation's performance under electrical stress.

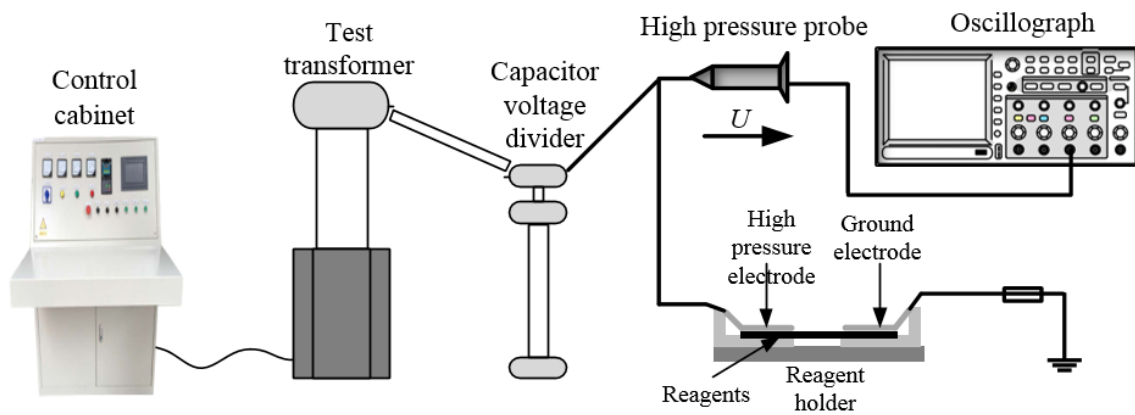


Figure 2. Test platform of AC discharge along the surface.

(3) Water contact angle test: The water contact angle test platform is shown in Figure 3. The temperature indicator patch sample to be measured was placed on the sample table of the water contact angle measuring instrument, the position of the sample was adjusted so that the acquisition system could obtain a clear image, and the injection unit was triggered to make the liquid drop fall on the surface of the sample. The water contact angle data were obtained by using the automatic ellipse fitting method. Ten locations were measured for each group of samples, and the average water contact angle was obtained after removing the maximum and minimum values.

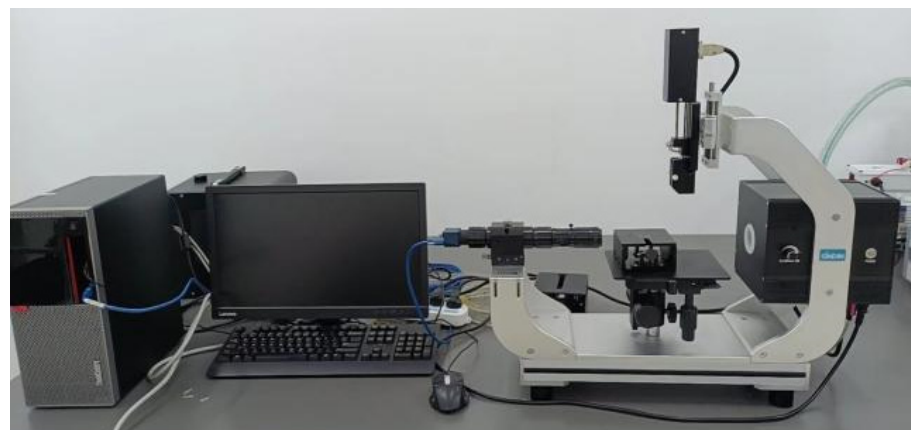


Figure 3. Test platform of water contact angle test.

3. Results and Discussion

3.1. Color-Changing Property

3.1.1. Color-Changing Effect

Figure 4 is the color change diagram of the reversible temperature indicator patch at different temperatures. The results show that the temperature range of the color change of the temperature indicator patch with a mass ratio of 1:2:50 is 49~55 °C, and the color changes from dark blue to gray, with an obvious color change effect. According to the standard DL/T 664-2016 infrared diagnostic application specification for live equipment, the temperature variation interval has a high matching degree with the thermal defect temperature at the lap surface of the transformer bushing head, and can better meet the requirements of abnormal temperature detection at the lap surface of the transformer bushing head.

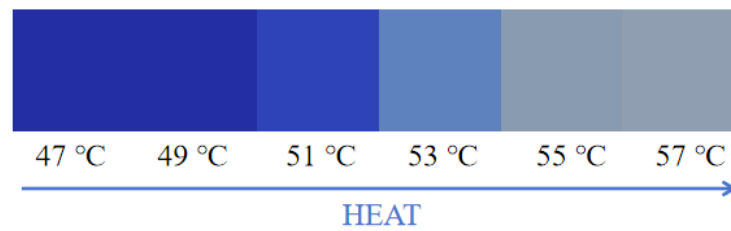
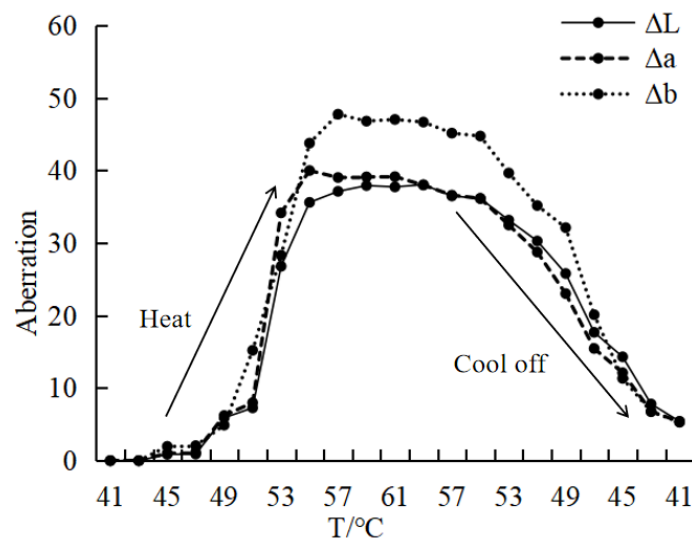


Figure 4. Color changes at different temperatures.

Figure 5 illustrates the variation in the color difference (ΔE) of the reversible temperature-indicating patch across different thermal conditions, employing ΔE as a metric to delineate the fading-color range. A significant shift in ΔE from its baseline at a specific temperature denotes the onset of color transformation. As can be seen from Figure 5a, the color difference values of the brightness index difference ΔL , red and green axis color index difference Δa , and yellow and blue axis color index difference Δb increase with the increase in temperature, and the value changes little before 49 °C, when the corresponding patch color does not fade significantly. When the heating temperature reaches 49 °C, the change rates of ΔL , Δa , and Δb increase significantly, and the surface color of the patch gradually disappears. When the temperature reaches 55 °C, ΔL , Δa , and Δb tend to be stable. After cooling, ΔL , Δa , and Δb continue to decrease, but their rate of decrease is slower than that of heating up. It can be seen from Figure 5b that the variation trend in the color difference ΔE is basically consistent with that of ΔL , Δa , and Δb , and there are obvious differences in the heating and cooling processes, indicating that the patch has a thermal hysteresis effect in the cooling process.



(a) ΔL , Δa , Δb

Figure 5. Cont.

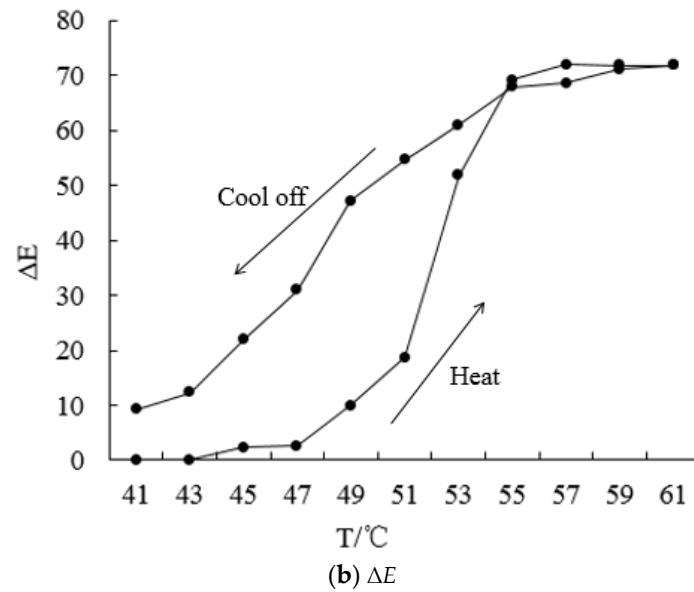


Figure 5. Colorimetric parameters of a thermographic patch at different temperatures.

The reversible patch exhibits a fading-temperature range of 49~55 °C and a color transition interval of 45~55 °C, shifting distinctly from dark blue to gray. This behavior aligns closely with the thermal defect temperatures on transformer bushing lap surfaces, as specified by the DL/T 664-2016 standard for infrared diagnostic applications on live equipment. Such compatibility underscores the patch's potential for enhancing the detection of abnormal thermal conditions on transformer bushing lap surfaces.

3.1.2. Color-Changing Time

The sensitivity of color change of the temperature-indicating patch is an indicator of its responsiveness to external thermal stimuli; it is quantified by two key metrics: fading time and recovery time. These durations inversely correlate with color sensitivity: shorter fading and recovery periods signify a heightened sensitivity, denoting a quicker response to thermal changes. The test samples were heated at 70 °C and cooled at 25 °C, and the color difference ΔE changed with time to determine the color change time. Figure 6 delineates the temporal dynamics of color transformation for the reversible temperature-indicating patch, illustrating its efficiency in reacting to thermal variations.

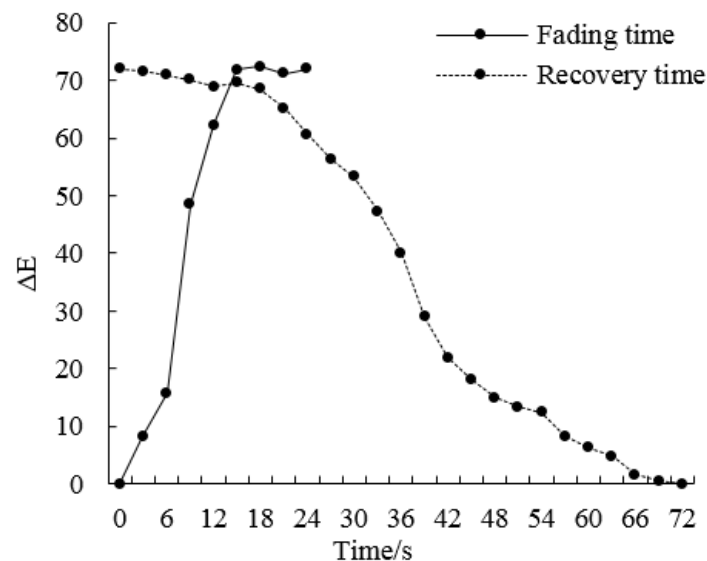


Figure 6. The color change time of the temperature-indicating patch.

Figure 6 reveals that the temperature-indicating patch has a rapid discoloration rate, with a fading time of 15 s, demonstrating high sensitivity and swift responsiveness to temperature fluctuations, particularly in the context of thermal defects on transformer bushing lap surfaces. Conversely, the patch's recovery time is significantly longer, at 69 s, indicating a slower recoloration process. This discrepancy can be attributed to several factors:

(1) The patch's composition, primarily octadecanol and a sealing layer film, exhibits low thermal conductivity and heat transfer rates, coupled with inefficient heat storage and release capabilities. These characteristics impede rapid heat dissipation, causing heat to linger within the patch after removal from the heat source, thus slowing the cooling process.

(2) Heat dissipation in the patch is predominantly through air convection and radiation, both of which are limited by the patch's small surface area and the inherent inefficiency of these mechanisms, further restricting heat exchange with the environment.

(3) The high heat capacity and latent heat of phase change of octadecanol, alongside significant heat absorption during the heating phase, necessitates extended durations for heat transfer during cooling. These findings underscore the complex interplay between material properties and thermal dynamics, influencing the patch's operational efficiency in real-world applications.

3.1.3. Reversibility of Discoloration

The reversible temperature indicator patch was subjected to cold- and hot-cycle tests at 25 °C and 70 °C. In order to ensure the complete discoloration of fading/recoloring, it was left for 3 min at each temperature. Figure 7 presents the variation in color difference (ΔE) of a reversible temperature-indicating patch subjected to 20 thermal cycles.

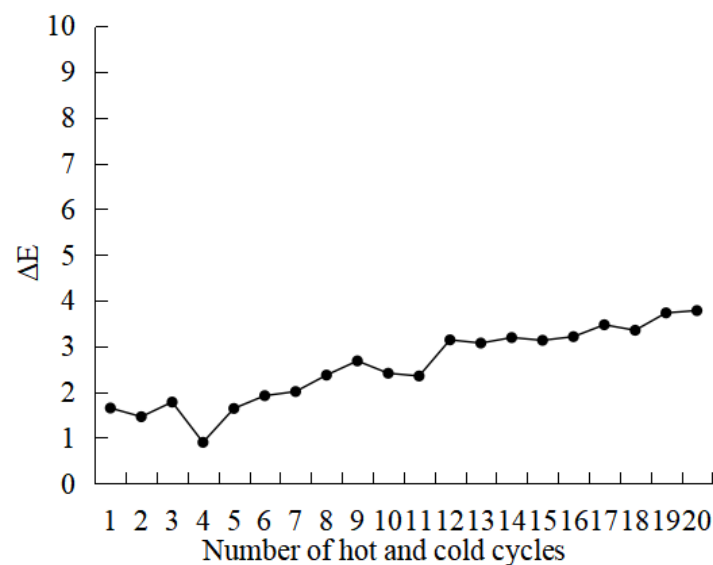


Figure 7. Total color difference ΔE of the hot- and cold-cycles of the temperature patch over 20 cycles.

The analysis reveals that ΔE fluctuates between 0.90 and 3.78 throughout these cycles, indicating a modest increasing trend with the progression of thermal cycling. However, when juxtaposed with the ΔE of 71.86 observed following complete discoloration, these values represent merely 1.25 to 5.26% of the total change, categorizing them within a minor color difference scope. This outcome attests to the exemplary reversibility of the devised temperature-indicating patch, confirming its efficacy for the in situ detection of thermal anomalies on the lap surface of transformer bushing head outlets.

3.2. Aging Performance of Temperature-Indicating Patch

3.2.1. Hydrophobicity

Figure 8 presents the variation in water contact angle for binder-based and vacuum-based temperature-sensitive patches subjected to thermal aging at 80 °C. As the aging

duration increases, a consistent decrease in the water contact angles of both patch types is observed. Specifically, the water contact angle for the binder-based patch diminishes from 89° to 80° , whereas for the vacuum-based patch it declines from 87° to 79° . Initially, the binder-based patch exhibits a higher water contact angle compared to the vacuum-based patch, indicating differences in their surface hydrophilicity due to their material compositions and structural characteristics. The reasons are as follows:

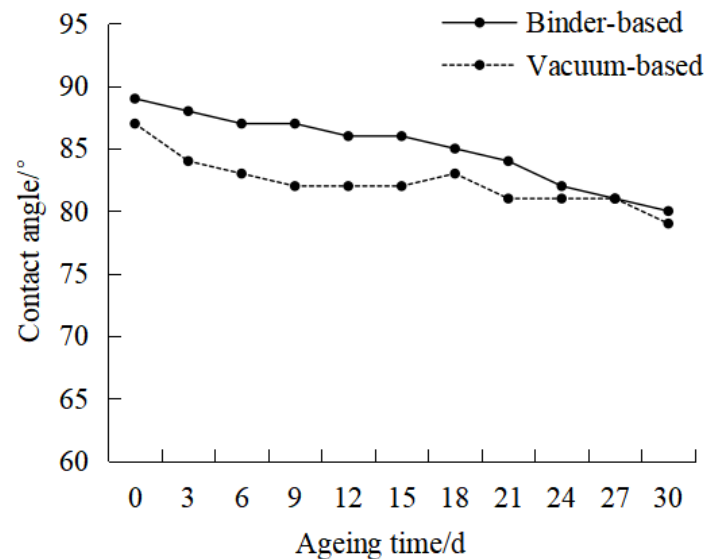


Figure 8. Temperature-indicating patch water contact angle change.

(1) The differential hydrophilic characteristics of binder-based and vacuum-based temperature-sensitive patches, initially, can be attributed to their distinct material compositions. The binder-based patch employs a polyethylene terephthalate (PET) film coating, characterized by a molecular structure with fewer polar groups, yielding relatively poor hydrophilicity and, consequently, a higher water contact angle. Conversely, the vacuum-based patch utilizes a sealing bag composed of a polyamide fiber (PA) and polyethylene (PE) blend, which, due to a higher concentration of polar groups in its molecular structure, exhibits better hydrophilicity and a lower initial water contact angle.

(2) During the thermal aging process, prolonged exposure to heat accelerates molecular motion on the material's surface, altering the arrangement and polarity distribution of surface molecules. This may lead to thermal cracking, degrading the surface microstructure and creating microgrooves or cracks aligned perpendicular to the direction of stress. These changes enhance the material's hydrophilicity, reducing the water contact angle over time. The intensification of chemical reactions and increased likelihood of thermal cracking with extended aging further contribute to the decreasing water contact angles observed in both types of temperature-sensitive patches.

3.2.2. Electrical Properties

Figure 9 demonstrates the effect of thermal aging duration on the flashover voltage per unit length across the surface of thermal patches. Compared to vacuum-based thermal patches, those of the adhesive type exhibit superior flashover voltage performance per unit length. As the aging period extends, a downward trend in flashover voltage per unit length is observed for both adhesive and vacuum types. After a 30-day aging period, the flashover voltage per unit length for adhesive-type thermal patches declines from 9.30 kV/cm to 8.93 kV/cm , a 3.98% decrease, while for vacuum-based, it reduces from 9.13 kV/cm to 8.59 kV/cm , representing a 5.91% decrease. The electrical performance of an adhesive temperature indicator patch is more stable than that of a vacuum-based. These results can be explained by the following reasons:

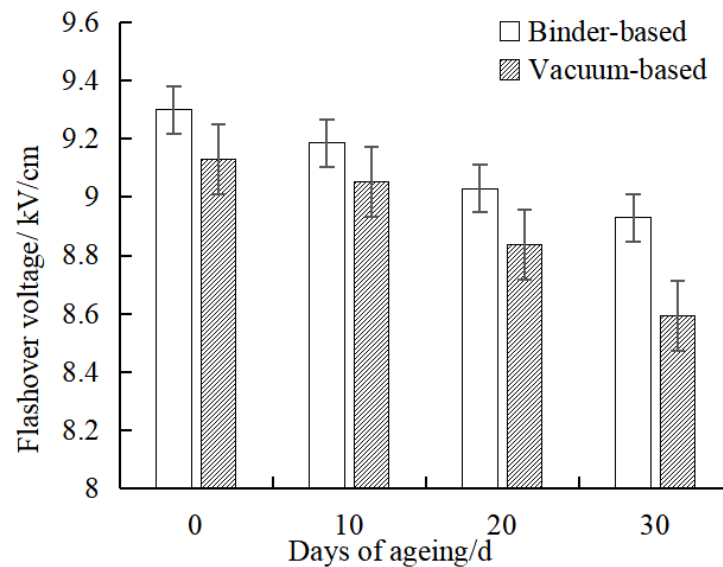


Figure 9. The flashover voltage per unit length of the temperature patch along the surface.

(1) The surface flashover voltage per unit length of temperature-sensitive patches is significantly influenced by their surface coatings. The binder-based patches, utilizing PET film, and the vacuum-based patches, employing a PA/PE mixed film, undergo physical and chemical aging during thermal exposure, leading to a decrease in their surface electrical strength. This decline can be explained by the theory of electronically triggered polarization relaxation, which posits that surface flashover initiates with the generation of primary electrons in areas of weak insulation. These electrons, propelled by the electric field towards the anode, collide with the material surface, spawning secondary electrons and leading to an electron avalanche that culminates in surface flashover discharge. Thermal aging exacerbates the situation by inducing thermal cracking and molecular chain segment rearrangement, thereby degrading the surface microstructure and promoting uneven electric field distribution due to surface irregularities. This results in enhanced local field strength distortion, initiating electron emission from weak insulation areas. As the aging process progresses, the surface deterioration intensifies. The contact between the surface of the temperature indicator patch and the electrode is poor, and there is a small gap. Electrical discharge occurs first inside the air gap, resulting in the generation of charged particles. The generated charged ions move along the surface of the solid medium, and the voltage distribution along the surface is not uniform, and it is easy for arc discharge to occur at high electric field intensities. On the other hand, the surface of the temperature-indicating patch is rough and uneven, resulting in uneven resistance distribution, distortion of the surface electric field, and a decrease in the flashover voltage along the surface.

(2) Furthermore, the differing compositions of the surface coatings play a critical role in their flashover voltages. The PET film, characterized by high corona resistance and insulation properties, exhibits a higher surface flashover voltage due to its ability to dissipate accumulated charge efficiently, attributed to its elevated conductivity and lower surface tension. In contrast, the PA/PE film, with its non-polar polymer composition and low surface energy, is more prone to electrostatic adsorption and charge accumulation, leading to a lower surface flashover voltage. Its high dielectric constant and low conductivity further hinder charge transfer, increasing susceptibility to flashover under equivalent voltage conditions.

4. Conclusions

The conclusions drawn are as follows.

(1) A temperature-sensitive display patch was fabricated using the melt processing technique, characterized by a transitional phase with a fading interval of 49~55 °C and a

reversible coloration span of 45~55 °C. This patch exhibits a pronounced chromatic transition, with the disappearance of color occurring within 15 s and color restoration taking approximately 69 s. Repeated thermal cycling tests, conducted 20 times, revealed a minimal variation in color difference (ΔE), ranging from 0.90 to 3.78. This represents a negligible proportion (1.25~5.26%) relative to the baseline color difference value of 71.86 observed upon complete color change. These findings underscore the patch's robust reversible functionality, affirming its potential for applications requiring precise temperature monitoring.

(2) With increasing thermal aging duration, the water contact angles of both binder-based and vacuum-based temperature-indicating patches exhibit a consistent decline. Specifically, the contact angle for binder-based patches decreases from 89° to 80°, whereas for vacuum-based patches, it falls from 87° to 79°. Notably, the binder-based patches demonstrate superior flashover voltage per unit length compared to their vacuum-based counterparts, indicating enhanced electrical insulation properties. However, as aging progresses, both types of patches show a diminishing trend in flashover voltage per unit length, with reductions of 3.98% for binder-based and 5.91% for vacuum-based patches, respectively. This suggests that, despite a general decline in electrical performance over time, binder-based patches maintain relative stability in their electrical properties when compared to vacuum-based patches.

Author Contributions: Conceptualization, X.W.; methodology, N.J.; experiment, W.J. and C.L.; writing—original draft preparation, M.W. and R.X. All authors have read and agreed to the published version of the manuscript.

Funding: This work was supported by the Shandong Electric Power Company's Science and Technology Project "Self-detection Method and Demonstration Application of Substation Primary Equipment Temperature Based on Reversible Colour Change Coating" (520607230004).

Data Availability Statement: The data presented in this study are available on request from the corresponding author.

Conflicts of Interest: Mingqin Wang, Xiaobin Wu, Nan Jiang, and Chenghua Liu are employed by the State Grid Shandong Linyi power supply company. The remaining authors declare that the research was conducted in the absence of any commercial or financial relationships that could be construed as a potential conflict of interest. The authors declare that this study received funding from Shandong Electric Power Company's Science and Technology. The funder was involved in the study design, collection, analysis, interpretation of data, the writing of this article or the decision to submit it for publication.

References

- Zhang, L.; Wang, W.; Han, Y.; Sun, L.; Wu, H.; Mu, H. Intelligent Monitoring of transformer bushing based on Multi-dimensional Parameter composite sensing. *High Volt. Eng.* **2022**, *48*, 2934–2944.
- Henderson, C.N.; DeFrance, C.S.; Predecki, P.; McCloskey, T.V.; Truitt, E.; Hoffman, J.; Kumosa, M. Ballistic Fragmentation Confinement of Coated Brittle Transformer Bushing Models. *Int. J. Impact Eng.* **2018**, *122*, 363–373. [[CrossRef](#)]
- Zhu, W.; Mao, B.; Xie, Q. Rapid assessment method of post-earthquake mechanical properties of 1100 kV extra-high voltage transformer bushings. *High Volt. Eng.* **2022**, *48*, 4904–4914.
- Yang, Z.; He, C.; Xie, Q. Seismic performance and stiffening strategy of transformer bushings on sidewall cover plates. *J. Constr. Steel Res.* **2020**, *174*, 106268. [[CrossRef](#)]
- Christina, A.; Salam, M.; Rahman, Q.; Islam, A.; Wen, F.; Ang, S.; Hasan, S.; Voon, W. Investigation of failure of high voltage bushing at power transformer. *J. Electrost.* **2018**, *96*, 49–56. [[CrossRef](#)]
- Yuan, Z.; Sun, G.; Tang, H.; Gao, K.; Hu, J.; He, J. Types and Mechanisms of Condenser Transformer Bushing Failures. *IEEE Electr. Insul. Mag.* **2023**, *39*, 26–36. [[CrossRef](#)]
- Setayeshmehr, A.; Akbari, A.; Borsi, H.; Gockenbach, E. On-line monitoring and diagnoses of power transformer bushings. *IEEE Trans. Dielectr. Electr. Insul.* **2006**, *13*, 608–615. [[CrossRef](#)]
- Zhang, L.; Sun, L.; Wu, J.; Han, Y.; Wang, S.; Yang, C.; Shen, W.; Guo, C. Development of multi-parameter online monitoring equipment for EHV transformer bushing. *IET Sci. Meas. Technol.* **2020**, *14*, 98–103. [[CrossRef](#)]
- Liu, L.; Jiao, H.; Li, P.; Gu, L.; Guo, L. Case analysis of misjudgment of transformer bushing infrared temperature measurement defect. *J. State Grid Technol. Inst.* **2018**, *21*, 13–15.
- Shen, X.; Yu, X.; Wang, Y.; Cheng, L.; Wang, D.; Chen, J. Three-dimensional visualization scheme of infrared thermal temperature measurement data for substation electric power equipment. *High Volt. Eng.* **2021**, *47*, 387–395.

11. Li, X.; Tang, Y.; Zhan, J.; Ye, J.; Fan, X.; Li, L. Research on the application of fiber grating sensor in transformer multi-parameter intelligent monitoring. *Power Syst. Prot. Control* **2023**, *51*, 154–160.
12. Zhong, J.; Huang, J. Review of hot spot Temperature Measurement and Calculation Methods for Power Transformers. *Electr. Switch.* **2019**, *57*, 1–4.
13. Li, L.; Zhao, X.; Wang, B.; Yang, S.; Nie, Y.; Jiang, X. Color change mechanism and application of thermochromic transition metal complexes. *Mater. Guide* **2023**, *37*, 183–193.
14. Crosby, P.H.N.; Netravali, A.N. Green Thermochromic Materials: A Brief Review. *Adv. Sustain. Syst.* **2022**, *6*, 2200208. [[CrossRef](#)]
15. Hakami, A.; Srinivasan, S.S.; Biswas, P.K.; Krishnegowda, A.; Wallen, S.L.; Stefanakos, E.K. Review on thermochromic materials: Development, characterization, and applications. *J. Coat. Technol. Res.* **2022**, *19*, 377–402. [[CrossRef](#)]
16. Dong, B.; Wu, B.; Meng, Y. Preparation and discoloration physicochemical properties of reversible thermochromic coatings for thermally induced defects in dry-type hollow reactors. *High Volt. Technol.* **2023**, *32*, 1–9.
17. Chen, Y. Research on temperature-demonstrating coatings for thermal fault detection in power systems. *Harbin Inst. Technol.* **2019**, *01*, 1–20.
18. Wang, P.; Zhang, X.; Chen, T.; Zhao, H. Preparation of superhydrophobic reversible thermochromic smart temperature—Sensitive coating and study of its performance. *Chin. J. Electr. Eng.* **2023**, *43*, 3642–3651.
19. Zhou, R.; Huang, H.; Shen, Q.; Liu, Z. Preparation of one-component thermo-reversible thermochromic coatings. *China Coat.* **2009**, *24*, 47–50.
20. Bhattacharya, R.; Ray, M.S.; Dey, R.; Righi, L.; Bocelli, G.; Ghosh, A. Synthesis, crystal structure and thermochromism of benzimidazolium tetrachlorocuprate: $(C_7H_7N_2)_2[CuCl_4]$. *Polyhedron* **2002**, *21*, 2561–2565. [[CrossRef](#)]
21. *DL/T 664-2016*; Application Rules of Infrared Diagnosis for Live Electrical Equipment. National Energy Administration of China: Beijing, China, 2016.
22. Zhang, R.; Lu, Y.; Xia, D. Modulation method for LED visible light communication based on uniform color space. *Laser J.* **2021**, *42*, 134–138.
23. Peng, Z.; Liu, Z.; Dou, H.; Guo, Z. ViBe motion target detection algorithm based on adaptive Lab color difference threshold. *Optoelectron. Laser* **2019**, *30*, 529–535.
24. *GB 11026.1-1989*; Guide for the Determination of Thermal Endurance Properties of Electrical Insulating Materials General Guidelines for Ageing Procedures and Evaluation of Test Results. Ministry of Machinery and Electronics Industry of the People's Republic of China: Beijing, China, 1989.
25. *GB/T 1408.1-2016*; Insulating Materials-Test Methods for Electric Strength-Part 1: Test at Power Frequencies. Standardization Administration of China: Beijing, China, 2016.

Disclaimer/Publisher's Note: The statements, opinions and data contained in all publications are solely those of the individual author(s) and contributor(s) and not of MDPI and/or the editor(s). MDPI and/or the editor(s) disclaim responsibility for any injury to people or property resulting from any ideas, methods, instructions or products referred to in the content.